Effect of the variation of electric-dipole moments on the shape of pressure-broadened atomic spectral lines

N. F. Allard
Observatoire de Paris-Meudon, Département Atomes et Molécules en Astrophysique, 92195 Meudon Principal Cedex, France and CNRS Institut d'Astrophysique, 98 bis Boulevard Arago, 75014 Paris, France

A. Royer
Département Génie Physique, Ecole Polytechnique, Montréal, Québec, Canada H3C3A7

J. F. Kielkopf
Department of Physics, University of Louisville, Louisville, Kentucky 40292

N. Feautrier
Observatoire de Paris-Meudon, Département Atomes et Molécules en Astrophysique, 92195 Meudon Principal Cedex, France
(Received 30 March 1999)

We derive a classical path expression for a pressure-broadened atomic spectral line shape that allows for an electric-dipole moment that is dependent on the position of perturbers. The theory is applied to the atomic hydrogen Lyman-α and Lyman-β lines broadened by collisions with neutral and ionized atomic hydrogen. The far wings of the Lyman series lines exhibit satellites, enhancements that may be associated with quasimolecular states of H_2 and H_2^+. The sizes of these features depend on the values of the electric-dipole moments at the internuclear separations responsible for the satellites. Profiles are computed with and without spatial dependence of the dipole moment, and are compared with astronomical and laboratory observations. We conclude that in the present case the variation of the dipole moment is an important factor that cannot be neglected. [S1050-2947(99)10308-1]

PACS number(s): 32.70.Jz, 52.25.Qt, 95.30.Dr, 95.30.Ky

I. INTRODUCTION

The aim of this paper is to provide a classical path theory for the shape of pressure-broadened atomic spectral lines that takes into account the variation of the electric-dipole moment during a collision. Anderson and Talman [1] developed a theory of spectral line pressure broadening in which the profile is given by the Fourier transform of an autocorrelation function. Their formalism has been widely followed in neutral atom line broadening theory, usually with the assumption that the electric-dipole moment during a collision is the same as it is for infinite separation of the emitting atom and its perturber. However, the electric-dipole moment is *not* constant. Accurate calculations of atomic hydrogen interactions show, for example, that the electric-dipole transition moments in H_2 may differ from asymptotic values by a factor more than 2 at interatomic separations of a few Å. Furthermore, both observations and theory of alkali atom spectra broadened by noble gases show that collisions alter the transition probability of forbidden transitions [2–7]. There is therefore theoretical and experimental evidence that for quantitative comparisons of line shape theory and observations to be meaningful, it is necessary to include the dependence of the electric-dipole moment on interatomic separation.

The far line wing generally does not decrease monotonically with increasing frequency separation from the line center. When the difference between the upper and lower interatomic potentials for a given transition goes through an extremum, a relatively wider range of interatomic distances contribute to the same spectral frequency, resulting in an enhancement, or *satellite*, in the line wing. Satellites in alkali atom spectra have been known since the 1930's [8]. The importance of this effect is highlighted by the recent discovery that the wings of Lyman-α and Lyman-β seen in stars and in laboratory plasmas show satellites associated with the molecular interactions of H_2 and H_2^+. The quasimolecular states that give rise to these satellites are transient, they occur during binary collisions with another neutral atom or a proton. With theoretical line models based on statistical arguments, Stewart, Peek, and Cooper [9] predicted that a satellite due to quasimolecular H_2^+ would enhance the Lyman-α wing at 1405 Å, and Sando, Doyle, and Dalgarno [10] found a satellite due to quasimolecular H_2 at 1623 Å.

The satellite lines at 1405 and 1623 Å were identified by Nelan and Wegner [11], and by Koester *et al.* [12] in ultraviolet spectra of white dwarf stars obtained by the International Ultraviolet Explorer (IUE) satellite. More recently, in 1995 high-quality spectra covering the range 820–1840 Å were obtained with the Hopkins Ultraviolet Telescope (HUT) for white dwarfs hotter than about 20 000 K. Absorption features in the wing near 1060 and 1078 Å were identified in the Lyman-β profile of the DA white dwarf Wolf 1346 as satellites due to quasimolecular H_2^+ [13]. The strengths of these satellite features and indeed the entire shape of wings in the Lyman series are very sensitive to the degree of ionization in the stellar atmosphere, because that determines the relative importance of broadening by ion and neutral collisions. When the spectral line profiles for the Lyman series are included as a source of opacity in model at-

mospheres for a white dwarf, a comparison of the predicted spectrum with the observed one permits an accurate determination of the temperature of the star.

The spectrum of light escaping from a white dwarf also controls the rate at which it cools. This rate may be predicted from a model for the atmosphere and opacity of the star, and consequently the temperature of a white dwarf star indicates its age [14,15]. This bears on issues of importance for cosmology because white dwarfs in our galaxy may be a source of microlensing events [14], and because the ages of the oldest white dwarfs may be used to set an upper limit on the age of the universe [15].

It is then very important to get an accurate quantitative determination of the satellite profiles. The approach we use is based on the quantum theory of spectral line shapes of Baranger [16,17] that were developed in an *adiabatic representation* to include the degeneracy of atomic levels [18,19]. However, because we are mostly interested in the line wings, we neglect transitions between asymptotically degenerate atomic states; that is, we perform an adiabatic approximation at the binary collision level. This approximation is expected to induce errors mostly in the shift of the line center, which is largely due to weak collisions involving the region where different (but asymptotically equal) potential curves merge together [20]. We then perform a classical path approximation within that framework. We apply this theory to the Lyman series of atomic hydrogen, and present calculations of profiles for Lyman-α and Lyman-β that take into account the dependence of the electric-dipole moment on internuclear distance during the collision. The resulting profiles show that the amplitude of satellites depends on the strength of the dipole moment in the region of internuclear distance where the satellite is formed.

Previous calculations of profiles used the approximation of replacing the electric-dipole transition moment by a constant [21–23]. They have been used successfully to evaluate synthetic spectra in the range of effective temperatures from about 20 000 down to 9000 K, which fit UV spectra of white dwarfs and λ Bootis stars quite well [24–27]. They also account for the spectra of laser-produced hydrogen plasmas [28,29]. However, the assumption of a constant dipole moment is questionable for allowed transitions, and does not even include the effects of collision-induced transitions which are asymptotically forbidden. To take this into account, we develop a general unified theory in which the dipole moment matrix element varies during a collision. The theory of the spectrum is presented in the following section.

We then evaluate the theory for Lyman-α and Lyman-β wings of H perturbed by protons. Both lines should really be treated simultaneously because the blue wing of Lyman-α and the red wing of Lyman-β overlap. However, we neglect interference terms between the two lines. The Lyman profiles and satellites are calculated for the physical conditions met in the atmospheres of white dwarfs, where low densities allow us to use an expansion of the autocorrelation function in powers of density as described in [30]. The profiles presented here use accurate theoretical molecular potentials to describe the interaction between radiator and perturber. H_2^+ potentials are taken from the tables of Madsen and Peek [31]. Dipole transition moments are those calculated by Ramaker and Peek [32].

We also apply the improved theory to the Lyman-α line broadened simultaneously by H-H and H-H^+ collisions. A comparison with laboratory experiments and astronomical observations demonstrates that the dipole moment variation is an important effect. The H_2 potentials contributing to Lyman-α are taken from Sharp [33] and Wolniewicz and Dressler [34]. The dipole moments of Dressler and Wolniewicz [35] were used for the transitions between the singlet quasimolecular states, and *ab initio* results of Drira [36] were used for the transitions between the triplet states.

II. GENERAL EXPRESSION FOR THE SPECTRUM

We consider a gas of atoms interacting with the radiation field. The power radiated at the frequency ω is written

$$P(\omega)=\frac{4\omega^4}{3c^3}I(\omega), \tag{1}$$

where c is the velocity of light and $I(\omega)$ is referred to as the spectrum [37]. In the dipole approximation, and neglecting Doppler effects, it is given by

$$I(\omega)=\sum_{n,n'}\delta(\omega-\omega_{nn'})|\langle n'|\mathbf{D}|n\rangle|^2\rho_n. \tag{2}$$

The summations extend over all states of the gas, each term weighted with the probability ρ_n for the initial state. **D** is the total dipole moment (we use bold notation for operators). $|n\rangle$ are eigenstates of **H**, the total Hamiltonian of the gas,

$$\mathbf{H}=\mathbf{T}_{nucl}+\mathbf{T}_{elec}+V(\mathbf{x},\mathbf{R}), \tag{3}$$

where $\mathbf{T}_{nucl}$ and $\mathbf{T}_{elec}$ are sums of nuclear and electronic kinetic-energy operators, respectively, and $V(\mathbf{x},\mathbf{R})$ is the interaction between particles. Here **x** denotes collectively the set of electronic coordinates (position and spin) plus spin coordinates of the nuclei, while **R** denotes the set of position coordinates of all the nuclei of the gas. ρ is the density matrix,

$$\rho\equiv\frac{e^{-\beta\mathbf{H}}}{\mathrm{Tr}\,e^{-\beta\mathbf{H}}}, \tag{4}$$

where β is the inverse temperature $(1/kT)$.

The spectrum $I(\omega)$ can be written as the Fourier transform of the dipole autocorrelation function $\Phi(s)$,

$$I(\omega)=\frac{1}{\pi}\mathrm{Re}\int_0^{+\infty}\Phi(s)e^{-i\omega s}ds. \tag{5}$$

Here,

$$\Phi(s)=\mathrm{Tr}\,\rho\mathbf{D}^\dagger e^{is\mathbf{H}/\hbar}\mathbf{D}e^{-is\mathbf{H}/\hbar} \tag{6}$$

$$=\langle\mathbf{D}^\dagger(0)\mathbf{D}(s)\rangle \tag{7}$$

is the autocorrelation function of the dipole moment in the Heisenberg representation [8],

$$\mathbf{D}(s)\equiv e^{is\mathbf{H}/\hbar}\mathbf{D}e^{-is\mathbf{H}/\hbar}. \tag{8}$$

We use the notation

$$\langle(\,)\rangle \equiv \mathrm{Tr}\,\rho(\,), \tag{9}$$

where Tr denotes the trace operation.

III. ADIABATIC REPRESENTATION

The adiabatic or Born-Oppenheimer representation comprises expanding states of the gas in terms of electronic states $\chi_e(x;R)$ corresponding to frozen nuclear configurations. In the Schrödinger equation

$$[\mathbf{T}_{elec}+V(\mathbf{x},\mathbf{R})]\chi_e(x;R)=\mathbf{H}_{elec}(R)\chi_e(x;R) \tag{10}$$

$$=E_e(R)\chi_e(x;R), \tag{11}$$

R appears as a parameter, and the eigenenergies $E_e(R)$ play the role of potential energies for the nuclei. The electronic states $\chi_e(x;R)$ form a complete orthonormal set in x space at each value of R. These states are called *adiabatic* because $\chi_e(x;R)$ follows *adiabatically* the motion of the nuclear coordinate R. We precede R with a '';'' to emphasize its role as a parameter. Any wave function $\Psi(x,R)$ can be expanded as

$$\Psi(x,R)=\sum_e \psi_e(R)\chi_e(x;R), \tag{12}$$

$$\psi_e(R)\equiv\int dx\,\chi_e(x;R)^*\Psi(x,R). \tag{13}$$

As the nuclei get further away from each other, which we denote by $R\to\infty$, the electronic energies $E_e(R)$ tend to asymptotic values E_e^∞, which are sums of individual atomic energies. Since atomic states are usually degenerate, there are in general several different energy surfaces that tend to a same asymptotic energy as $R\to\infty$. Let us denote by E_j^∞ the asymptotic energies and call ε_j the subspace of electronic states $\chi_e(x;R)$ such that $E_e(R)\to E_j^\infty$ as $R\to\infty$.

From now on, consider specifically a single radiating atom, the *radiator*, immersed in a gas of optically inactive atoms, the *perturbers*. For a transition $\alpha=(i,f)$ from initial state i to final state f, we have R-dependent frequencies

$$\omega_{e'e}(R)\equiv[E_{e'}(R)-E_e(R)]/\hbar,\quad e\in\varepsilon_i,\quad e'\in\varepsilon_f, \tag{14}$$

which tend to the isolated radiator frequency

$$\omega_\alpha\equiv\omega_{fi}\equiv(E_f^\infty-E_i^\infty)/\hbar \tag{15}$$

as the perturbers get sufficiently far from the radiator:

$$\omega_{e'e}(R)\to\omega_{fi}\quad\text{as}\quad R\to\infty,\quad e\in\varepsilon_i,\quad e'\in\varepsilon_f. \tag{16}$$

Let us introduce projectors $\mathbf{P}_e$, which select the e^{th} adiabatic component of any $\Psi(x,R)$ according to [19]

$$\mathbf{P}_e\Psi(x,R)=\psi_e(R)\chi_e(x;R). \tag{17}$$

Let $\mathbf{P}_j=\Sigma_{e\in\varepsilon_j}\mathbf{P}_e$ be the projector onto the subspace ε_j of electronic states of asymptotic energy E_j^∞. We write the dipole moment as a sum over transitions

$$\mathbf{D}=\sum_\alpha \mathbf{D}_\alpha, \tag{18}$$

$$\mathbf{D}_\alpha\equiv\sum_{e,e'}^{(\alpha)}\mathbf{P}_{e'}\mathbf{D}\mathbf{P}_e. \tag{19}$$

In the Heisenberg representation

$$\mathbf{D}_\alpha(t)\equiv\sum_{e,e'}^{(\alpha)} e^{it\mathbf{H}/\hbar}\mathbf{P}_{e'}\mathbf{D}\mathbf{P}_e e^{-it\mathbf{H}/\hbar}, \tag{20}$$

$$\equiv\sum_{e,e'}^{(\alpha)}\mathbf{D}_{e'e}(t). \tag{21}$$

The sum $\Sigma_{e,e'}^{(\alpha)}$ is over all pairs (e,e') such that $\omega_{e',e}(R)\to\omega_\alpha$ as $R\to\infty$. Thus $\mathbf{D}_\alpha$ connects all pairs of adiabatic states whose electronic energy differences become equal to ω_α as $R\to\infty$. In the absence of perturbers, $\mathbf{D}_\alpha$ would be the component of $\mathbf{D}$ responsible for the radiative transitions of frequency ω_α.

The $(R\to\infty)$ degeneracy of a subspace ε_j is usually due to rotational invariance, and is therefore of multiplicity $(2J_j+1)$, where J_j is the total angular momentum of the radiator as $R\to\infty$ (when perturbers are close to the radiator, the angular momentum of the radiator is not a good quantum number, and it can be defined in only an approximate manner). We note that the projection operators account for the weighting factors discussed in Ref. [23].

IV. CORRELATION AND SPECTRAL MATRICES

Introducing the expansion Eq. (18) for $\mathbf{D}$ into the expression Eq. (7) for $\Phi(s)$, we obtain

$$\Phi(s)=\sum_{\alpha,\beta}\Phi_{\alpha,\beta}(s), \tag{22}$$

where

$$\Phi_{\alpha,\beta}(s)=\mathrm{Tr}\,\rho\mathbf{D}_\alpha^\dagger e^{is\mathbf{H}/\hbar}\mathbf{D}_\beta e^{-is\mathbf{H}/\hbar} \tag{23}$$

$$=\langle\mathbf{D}_\alpha^\dagger(0)\mathbf{D}_\beta(s)\rangle. \tag{24}$$

The line shape is then

$$I(\omega)=\sum_{\alpha,\beta}I_{\alpha,\beta}(\omega). \tag{25}$$

It is convenient to think of the $\Phi_{\alpha,\beta}$ and $I_{\alpha,\beta}$ as elements of two matrices, which we may call the correlation and spectral matrices, respectively. The off-diagonal terms $I_{\alpha,\beta}(\omega)$, $\alpha\neq\beta$, represent interference between different spectral lines [17], arising, for instance, from avoided crossings between potential curves with different values E_e^∞. We shall neglect these interference terms. Then

$$I(\omega)=\sum_\alpha I_\alpha(\omega) \tag{26}$$

and

$$\Phi(s)=\sum_{\alpha}\Phi_{\alpha}(s), \tag{27}$$

where

$$\Phi_{\alpha}(s)=\langle \mathbf{D}_{\alpha}^{\dagger}(0)\mathbf{D}_{\alpha}(s)\rangle. \tag{28}$$

A. Zero-perturber spectrum

Using superscripts $(0),(1),\ldots,(N)$ to mean that $0,1,\ldots,N$ perturbers are present in a (large) volume $\mathcal{V}$ around the radiator, we write the zero-perturber correlation function as

$$\Phi_{\alpha}^{(0)}(s)=\phi_{\alpha}^{(0)}e^{i\omega_{\alpha}s}, \tag{29}$$

where

$$\phi_{\alpha}^{(0)}=\Phi_{\alpha}^{(0)}(s=0)=\langle \mathbf{D}_{\alpha}^{\dagger}\mathbf{D}_{\alpha}\rangle^{(0)} \tag{30}$$

$$=\sum_{e,e'}^{(\alpha)}\rho_e|\mathbf{D}_{ee'}^{(0)}|^2 \tag{31}$$

is the line strength, and where $\Sigma_{e,e'}^{(\alpha)}$ sums over pairs (e,e') such that $\omega_{e',e}(R\rightarrow\infty)=\omega_{\alpha}$, the frequency of the isolated radiator.

B. Interaction representation

The time dependence of $\Phi_{\alpha}(s)$ is determined by $\mathbf{D}_{\alpha}(s)$, the part of the dipole moment which, in the absence of perturbers, oscillates at the frequency ω_{α}. It is convenient to express $\Phi_{\alpha}(s)$ in a kind of *interaction representation* by dividing out its zero-perturber behavior. We thus write

$$\Phi_{\alpha}(s)=\phi_{\alpha}^{(0)}e^{i\omega_{\alpha}s}\Psi_{\alpha}(s), \tag{32}$$

where the interaction representation correlation function

$$\Psi_{\alpha}(s)\equiv\frac{\Phi_{\alpha}(s)}{\Phi_{\alpha}^{(0)}(s)} \tag{33}$$

contains all the influence of the perturbers on line α. Note that in the absence of perturbers we have

$$\Psi_{\alpha}^{(0)}(s)=1. \tag{34}$$

V. UNCORRELATED PERTURBERS APPROXIMATION

We now assume that the effects of the different perturbers on the line shape are uncorrelated (see Ref. [19] for a general discussion); that is, we approximate $\Psi_{\alpha}^{(N)}(s)$ by

$$\Psi_{\alpha}^{(N)}(s)=[\Psi_{\alpha}^{(1)}(s)]^N, \tag{35}$$

where N is the number of perturbers in the large volume $\mathcal{V}$, and $\Psi_{\alpha}^{(1)}(s)$ corresponds to the presence of a single perturber in $\mathcal{V}$. Now, $\Psi_{\alpha}^{(1)}(s)$ differs from the zero-perturber value $\Psi_{\alpha}^{(0)}(s)=1$ only if the single perturber interacts with the radiator during the time interval $(0,s)$, the probability for which is proportional to $1/\mathcal{V}$. So

$$\Psi_{\alpha}^{(1)}(s)=1+\frac{1}{\mathcal{V}}f_{\alpha}(s), \tag{36}$$

where

$$f_{\alpha}(s)=\mathcal{V}[\Psi_{\alpha}^{(1)}(s)-1] \tag{37}$$

is well defined as $\mathcal{V}\rightarrow\infty$. We thus get

$$\Psi_{\alpha}^{(N)}(s)=\left(1+\frac{1}{N}\frac{N}{\mathcal{V}}f_{\alpha}(s)\right)^N. \tag{38}$$

In the limit $N\rightarrow\infty$, $\mathcal{V}\rightarrow\infty$, with $N/\mathcal{V}=n$, the perturber number density, we get

$$\Psi_{\alpha}^{(N)}(s)=e^{nf_{\alpha}(s)}. \tag{39}$$

Let us now denote

$$\mathbf{d}_{\alpha}(s)\equiv\mathbf{D}_{\alpha}(s)e^{-i\omega_{\alpha}s}, \tag{40}$$

wherein the free evolution $e^{-i\omega_{\alpha}s}$ is factored out. Then,

$$f_{\alpha}(s)=\mathcal{V}\left(\frac{\Phi_{\alpha}^{(1)}(s)}{\Phi_{\alpha}^{(0)}(s)}-1\right) \tag{41}$$

$$=\mathcal{V}\left(\frac{\langle \mathbf{d}_{\alpha}^{(1)\dagger}(0)\mathbf{d}_{\alpha}^{(1)}(s)-\mathbf{d}_{\alpha}^{(0)\dagger}\mathbf{d}_{\alpha}^{(0)}\rangle}{\phi_{\alpha}^{(0)}}\right), \tag{42}$$

where we used Eq. (30). We note that $\Psi_{\alpha}(0)\neq 1$, and correspondingly

$$f_{\alpha}(0)=\mathcal{V}[\Psi_{\alpha}^{(1)}(0)-1] \tag{43}$$

$$=\mathcal{V}\frac{\langle \mathbf{d}_{\alpha}^{(1)^2}-\mathbf{d}_{\alpha}^{(0)^2}\rangle}{\langle \mathbf{d}_{\alpha}^{(0)^2}\rangle}\neq 0. \tag{44}$$

Thus the perturbed line strength $\phi_{\alpha}^{(0)}e^{nf_{\alpha}(0)}$ differs from the *free* line strength $\phi_{\alpha}^{(0)}$ by the factor $e^{nf_{\alpha}(0)}$. This density-dependent factor expresses the fact that the total intensity radiated increases or decreases according as the dipole moment is increased or decreased, on average, by the proximity of perturbers [$e^{nf_{\alpha}(0)}$ corresponds to the factor $e^{n\langle d^2-1\rangle}$ in Eq. (2.15) of Ref. [38], where the nondegenerate case was treated]. Let us write

$$f_{\alpha}(s)=f_{\alpha}(0)+g_{\alpha}(s), \tag{45}$$

where

$$g_{\alpha}(s)=f_{\alpha}(s)-f_{\alpha}(0) \tag{46}$$

$$=\mathcal{V}\frac{\langle \mathbf{d}_{\alpha}^{(1)\dagger}(0)[\mathbf{d}_{\alpha}^{(1)}(s)-\mathbf{d}_{\alpha}^{(1)}(0)]\rangle}{\langle \mathbf{d}_{\alpha}^{(0)^2}\rangle}. \tag{47}$$

Noting that $g_{\alpha}(0)=0$, we define a *normalized lineshape*

$$J_{\alpha}(\Delta\omega)=\frac{1}{\pi}\mathrm{Re}\int_0^{+\infty}e^{ng_{\alpha}(s)}e^{-i\Delta\omega s}ds, \tag{48}$$

where $\Delta\omega=\omega-\omega_\alpha$ is the frequency measured relative to the unperturbed line. Combining the above results for a pair of lines, such as Lyman-α and Lyman-β, we have

$$\Phi(s)=\Phi_\alpha(s)+\Phi_\beta(s) \tag{49}$$

$$=\phi_\alpha^{(0)}e^{i\omega_\alpha s}e^{nf_\alpha(s)}+\phi_\beta^{(0)}e^{i\omega_\beta s}e^{nf_\beta(s)}, \tag{50}$$

and

$$I(\omega)=\phi_\alpha^{(0)}e^{nf_\alpha(0)}J_\alpha(\omega-\omega_\alpha)+\phi_\beta^{(0)}e^{nf_\beta(0)}J_\beta(\omega-\omega_\beta). \tag{51}$$

Elimination of center-of-mass motion

Consider the zero-perturber quantity

$$\phi_\alpha^{(0)}=\left[\frac{\mathrm{Tr}\,e^{-\beta\mathbf{H}}\mathbf{d}_\alpha^\dagger\mathbf{d}_\alpha}{\mathrm{Tr}\,e^{-\beta\mathbf{H}}}\right]^{(0)}. \tag{52}$$

Since here $\mathbf{H}$ is a sum of the electronic Hamiltonian and the nuclear kinetic energy for the radiator alone, the *nuclear* components in Eq. (52) factor out in both the numerator and denominator, and cancel one another. Likewise, in Eq. (47),

$$\langle\mathbf{d}_\alpha^\dagger(0)[\mathbf{d}_\alpha(s)-\mathbf{d}_\alpha(0)]^{(1)}\rangle =\left[\frac{\mathrm{Tr}\,e^{-\beta\mathbf{H}}\mathbf{d}_\alpha^\dagger(0)[\mathbf{d}_\alpha(s)-\mathbf{d}_\alpha(0)]}{\mathrm{Tr}\,e^{-\beta\mathbf{H}}}\right]^{(1)}, \tag{53}$$

which refers to the radiator and a single perturber. The center-of-mass motion of the radiator-perturber pair factors out in both numerator and denominator, and cancels. Henceforth, we consider that Eq. (52) refers to the electronic motion of the radiator, and that Eq. (53) refers to the electronic and *relative* nuclear motion of the radiator-perturber pair. In other words, we can consider that the radiator is fixed at the origin with an infinite mass, and that the perturber has a mass equal to the reduced mass μ of the radiator perturber pair, where

$$\mu\equiv\frac{m_{rad}m_{pert}}{m_{rad}+m_{pert}}. \tag{54}$$

The electronic basis $\chi_e(x;\vec{r})$ in the case of a single perturber

We let $\vec{r}$ be the position vector of the perturber relative to the radiator. The $\chi_e(x;\vec{r})$ are stationary electronic states for fixed $\vec{r}$:

$$[\mathbf{T}_{elec}+V(\mathbf{x},\vec{r})]\chi_e(x;\vec{r})=E_e(r)\chi_e(x;\vec{r}). \tag{55}$$

The different electronic states correspond to different components of the electronic angular momentum about the internuclear axis $\vec{r}$. Now the total Hamiltonian is

$$\mathbf{H}=\mathbf{H}_{elec}+\mathbf{T}_{nucl}, \tag{56}$$

where

$$\mathbf{H}_{elec}=\mathbf{T}_{elec}+V(\mathbf{x},\vec{\mathbf{r}}). \tag{57}$$

Here, $\vec{\mathbf{r}}$ denotes the relative position operator, and

$$\mathbf{T}_{nucl}=\frac{\vec{\mathbf{p}}^2}{2\mu}, \tag{58}$$

where $\vec{\mathbf{p}}$ is the momentum operator for the relative motion of the radiator-perturber pair, so that

$$[\mathbf{r}_i,\mathbf{p}_j]=i\hbar\,\delta_{ij}. \tag{59}$$

Let $|\chi_e(\vec{\mathbf{r}})\rangle$ be a ket in the electronic subspace, and an *operator* in the nuclear subspace (hence $\mathbf{r}$ bold), defined by

$$\langle x|\chi_e(\vec{\mathbf{r}})\rangle=\chi_e(x;\vec{\mathbf{r}}), \tag{60}$$

so that

$$\langle\chi_{e'}(\vec{\mathbf{r}})|\chi_e(\vec{\mathbf{r}})\rangle=\delta_{e'e}, \tag{61}$$

and

$$\sum_e|\chi_e(\vec{\mathbf{r}})\rangle\langle\chi_e(\vec{\mathbf{r}})|=\mathbf{1}. \tag{62}$$

We have, in view of Eq. (55),

$$\langle\chi_{e'}(\vec{\mathbf{r}})|\mathbf{H}|\chi_e(\vec{\mathbf{r}})\rangle=E_e(\vec{\mathbf{r}})\,\delta_{ee'}+\left\langle\chi_{e'}(\vec{\mathbf{r}})\left|\frac{\vec{\mathbf{p}}^2}{2\mu}\right|\chi_e(\vec{\mathbf{r}})\right\rangle. \tag{63}$$

Now

$$\langle\chi_{e'}(\vec{\mathbf{r}})|\vec{\mathbf{p}}^2|\chi_e(\vec{\mathbf{r}})\rangle=\sum_{e''}\langle\chi_{e'}(\vec{\mathbf{r}})|\vec{\mathbf{p}}|\chi_{e''}(\vec{\mathbf{r}})\rangle\langle\chi_{e''}(\vec{\mathbf{r}})|\vec{\mathbf{p}}|\chi_e(\vec{\mathbf{r}})\rangle \tag{64}$$

and, in view of Eq. (59),

$$\langle\chi_{e''}(\vec{\mathbf{r}})|\vec{\mathbf{p}}|\chi_e(\vec{\mathbf{r}})\rangle=\delta_{e''e}\vec{\mathbf{p}}+\langle\chi_{e''}(\vec{\mathbf{r}})|[\vec{\mathbf{p}},\chi_e(\vec{\mathbf{r}})]\rangle \tag{65}$$

$$=\delta_{e''e}\vec{\mathbf{p}}-\frac{i\hbar}{\mu}\langle\chi_{e''}(\vec{\mathbf{r}})|\vec{\nabla}\chi_e(\vec{\mathbf{r}})\rangle \tag{66}$$

$$\equiv\delta_{e''e}\vec{\mathbf{p}}+\vec{\pi}_{e''e}(\vec{\mathbf{r}}) \tag{67}$$

so that [39]

$$\langle\chi_{e'}(\vec{\mathbf{r}})|\vec{\mathbf{p}}^2|\chi_e(\vec{\mathbf{r}})\rangle=\sum_{e''}[\vec{\mathbf{p}}\delta_{e'e''}+\vec{\pi}_{e'e''}(\vec{\mathbf{r}})]\times[\vec{\mathbf{p}}\delta_{e''e}+\vec{\pi}_{e''e}(\vec{\mathbf{r}})] \tag{68}$$

$$=\{[\vec{\mathbf{p}}+\vec{\pi}(\vec{\mathbf{r}})]^2\}_{e'e}. \tag{69}$$

The operator

$$\vec{\pi}_{e'e}(\vec{\mathbf{r}})=-\frac{i\hbar}{\mu}\langle\chi_{e'}(\vec{\mathbf{r}})|\vec{\nabla}\chi_e(\vec{\mathbf{r}})\rangle \tag{70}$$

leads to the usual radial and rotational coupling terms [40,41]. As we said above, the $|\chi_e(\vec{r})\rangle$ are referred to as the

internuclear axis, so they depend on $\vec{r}$ even at large distances, at which the electronic states are just products of atomic states. Let r_c be a distance beyond which electronic states are essentially products of atomic orbitals. When $r > r_c$, it is better to use a basis $|\chi_e(\vec{r})_z\rangle$ which is referred to as a fixed z axis. Let $\mathcal{R}$ be the rotation which rotates $\vec{r}$ to the z direction (that is, a rotation by some angle about the axis perpendicular to both $\vec{r}$ and z). The electronic bases, $|\chi_e(\vec{r})_z\rangle$ and $|\chi_e(\vec{r})_{\vec{r}}\rangle$ (referred to the internuclear axis $\vec{r}$) are connected to one another by means of the rotation operator $\mathcal{R}_{elec}$, which effects the rotation $\mathcal{R}$ in the *electronic* subspace. We thus choose the basis $|\chi_e(\vec{r})\rangle$ as follows:

$$|\chi_e(\vec{r})\rangle = |\chi_e(\vec{r})_{\vec{r}}\rangle \quad \text{for} \quad r < r_c$$

$$= \mathcal{R}_{elec}|\chi_e(\vec{r})_{\vec{r}}\rangle \quad \text{for} \quad r > r_c .$$

Note that both $E_e(\vec{r})$ and $|\chi_e(\vec{r})\rangle$ become independent of r at large r. In this way, for $r > r_c$, we have $\vec{\pi}_{ee'}(\vec{r}) = 0$, and Eq. (63) becomes, for $r > r_c$,

$$\langle \chi_{e'}(\vec{r})|\mathbf{H}|\chi_e(\vec{r})\rangle = \left(-\frac{\hbar^2 \nabla_r^2}{2\mu} + E_e^{\infty} \right) \delta_{e'e} \tag{71}$$

or

$$(\mathbf{H} - E_e^{\infty})|\chi_e(\vec{r})\rangle = |\chi_e(\vec{r})\rangle \frac{\vec{\mathbf{p}}^2}{2\mu}, \tag{72}$$

since $|\chi_{e'}(\vec{r})\rangle$ is a complete electronic basis. At smaller values of r, $\vec{\pi}_{e'e}(\vec{r}) \neq 0$. However, it is effective at inducing transitions only where the potential difference $E_{e'}(r) - E_e(r)$ is small; that is, near inner potential avoided crossings, and in the vicinity of r_c, where the different potential curves merge together.

A more explicit expression for $g_\alpha(s)$

Let us first evaluate the quantity $(\mathrm{Tr}\, e^{-\beta \mathbf{H}})^{(1)}$ appearing in Eq. (53), where the superscript (1) signifies as before that there is only one perturber present. Breaking up the trace into nuclear and electronic parts, we have

$$(\mathrm{Tr}\, e^{-\beta \mathbf{H}})^{(1)} = \sum_e e^{-\beta E_e^{\infty}} \mathrm{Tr}_r \langle \chi_e(\vec{\mathbf{r}})| e^{-\beta(\mathbf{H} - E_e^{\infty})}|\chi_e(\vec{\mathbf{r}})\rangle, \tag{73}$$

where we added factors $e^{-\beta E_e^{\infty}}$ and $e^{\beta E_e^{\infty}}$, which cancel one another. To simplify this notation we drop the superscript ∞ on E_e^{∞} $[E_e \equiv E_e(r \to \infty) = E_e^{\infty} = E_i]$. Now the part of $\mathrm{Tr}_r(\cdots) = \int d\vec{r} \langle \vec{r}|(\cdots)|\vec{r}\rangle$ coming from the interaction volume $\mathcal{V}_c = 4\pi r_c^3/3$ is negligible compared to the part coming from outside $\mathcal{V}_c$, which will turn out to be proportional to the large volume $\mathcal{V}$. Indeed, in view of Eq. (72) and since $\langle \chi_e(\vec{\mathbf{r}})|\chi_e(\vec{\mathbf{r}})\rangle = 1$, Eq. (73) is essentially equal to

$$(\mathrm{Tr}\, e^{-\beta \mathbf{H}})^{(1)} = \sum_e e^{-\beta E_e} \mathrm{Tr}_r e^{-\beta(\vec{\mathbf{p}}^2/2\mu)}. \tag{74}$$

Now,

$$\mathrm{Tr}_r e^{-\beta(\vec{\mathbf{p}}^2/2\mu)} = \int d\vec{p}\, e^{-\beta(\vec{p}^2/2\mu)} \langle \vec{p}|\vec{p}\rangle \tag{75}$$

$$= \frac{\mathcal{V}}{(2\pi\hbar)^3} \int d\vec{p}\, e^{-\beta(\vec{p}^2/2\mu)}, \tag{76}$$

where we used

$$\langle \vec{p}|\vec{p}\rangle = \int d\vec{r} \langle \vec{p}|\vec{r}\rangle \langle \vec{r}|\vec{p}\rangle \tag{77}$$

$$= \int d\vec{r} \frac{1}{(2\pi\hbar)^3} = \frac{\mathcal{V}}{(2\pi\hbar)^3}. \tag{78}$$

Thus

$$(\mathrm{Tr}\, e^{-\beta \mathbf{H}})^{(1)} = \frac{\mathcal{V}}{(2\pi\hbar)^3} \left(\int d\vec{p}\, e^{-\beta(\vec{p}^2/2\mu)} \right) \sum_e e^{-\beta E_e}. \tag{79}$$

We also need the results

$$(\mathrm{Tr}\, e^{-\beta \mathbf{H}})^{(0)} = \sum_e e^{-\beta E_e} \tag{80}$$

and

$$(\mathrm{Tr}\, e^{-\beta \mathbf{H}} \mathbf{d}_\alpha^\dagger \mathbf{d}_\alpha)^{(0)} = \sum_{e \in \varepsilon_i} \sum_{e' \in \varepsilon_f} e^{-\beta E_e} |d_{ee'}|^2 \tag{81}$$

$$= \sum_{e,e'}^{(\alpha)} e^{-\beta E_e} |d_{ee'}|^2 \tag{82}$$

$$= e^{-\beta E_i} \sum_{e,e'}^{(\alpha)} |d_{ee'}|^2. \tag{83}$$

Combining Eqs. (83), (80), (79), (53), (52), with Eq. (47), we get

$$g_\alpha(s) = \frac{\mathcal{V}}{\phi_\alpha^{(0)}} \left(\frac{(\mathrm{Tr}\, e^{-\beta \mathbf{H}} \mathbf{d}_\alpha^\dagger(0)[\mathbf{d}_\alpha(s) - \mathbf{d}_\alpha(0)])^{(1)}}{(\mathrm{Tr}\, e^{-\beta \mathbf{H}})^{(1)}} \right) \tag{84}$$

$$= \frac{(2\pi\hbar)^3}{\int dp e^{-\beta(\vec{p}^2/2\mu)}} \times \frac{\mathrm{Tr}\, e^{-\beta(\mathbf{H} - E_i)} \mathbf{d}_\alpha^{(1)\dagger}(0)[\mathbf{d}_\alpha^{(1)}(s) - \mathbf{d}_\alpha^{(1)}(0)]}{\sum_{e,e'}^{(\alpha)} |d_{ee'}^{(0)}|^2}. \tag{85}$$

Recalling the definition of $\mathbf{d}_\alpha$ in terms of the projectors

$$\mathbf{P}_i = \sum_{e \in \varepsilon_i} |\chi_e(\vec{\mathbf{r}})\rangle \langle \chi_e(\vec{\mathbf{r}})|, \tag{86}$$

$$\mathbf{P}_f=\sum_{e'\in\varepsilon_f}|\chi_{e'}(\vec{\mathbf{r}})\rangle\langle\chi_{e'}(\vec{\mathbf{r}})|, \tag{87}$$

putting

$$\omega_\alpha=\omega_{fi}=\frac{E_f^\infty-E_i^\infty}{\hbar}, \tag{88}$$

and using

$$e^{-is\omega_{fi}}=e^{isE_f/\hbar}e^{-isE_i/\hbar}, \tag{89}$$

we get

$$[\mathrm{Tr}\,e^{-\beta(\mathbf{H}-E_i)}\mathbf{d}_\alpha^\dagger(0)\mathbf{d}_\alpha(s)]^{(1)}=\mathrm{Tr}\,e^{-\beta(\mathbf{H}-E_i)}\mathbf{P}_i\mathbf{d}\mathbf{P}_f e^{is\mathbf{H}/\hbar}\mathbf{P}_f\mathbf{d}\mathbf{P}_i e^{-is\mathbf{H}/\hbar}e^{-is\omega_{fi}} \tag{90}$$

$$=\sum_{e,e'''\in\varepsilon_i}\sum_{e',e''\in\varepsilon_f}\mathrm{Tr}\,e^{-\beta(\mathbf{H}-E_i)}|\chi_e(\vec{\mathbf{r}})\rangle\langle\chi_e(\vec{\mathbf{r}})|\mathbf{d}|\chi_{e'}(\vec{\mathbf{r}})\rangle\langle\chi_{e'}(\vec{\mathbf{r}})|e^{is(\mathbf{H}-E_f)/\hbar}|\chi_{e''}(\vec{\mathbf{r}})\rangle$$
$$\times\langle\chi_{e''}(\vec{\mathbf{r}})|\mathbf{d}|\chi_{e'''}(\vec{\mathbf{r}})\rangle\langle\chi_{e'''}(\vec{\mathbf{r}})|e^{-is(\mathbf{H}-E_i)/\hbar} \tag{91}$$

$$=\sum_{e,e'''\in\varepsilon_i}\sum_{e',e''\in\varepsilon_f}\mathrm{Tr}_r d_{ee'}(\vec{\mathbf{r}})\langle\chi_{e'}(\vec{\mathbf{r}})|e^{\frac{is(\mathbf{H}-E_f)}{\hbar}}|\chi_{e''}(\vec{\mathbf{r}})\rangle d_{e''e'''}(\vec{\mathbf{r}})$$
$$\times\langle\chi_{e'''}(\vec{\mathbf{r}})|e^{-is(\mathbf{H}-E_i)/\hbar}e^{-\beta(\mathbf{H}-E_i)}|\chi_e(\vec{\mathbf{r}})\rangle. \tag{92}$$

Here Tr_r traces over $\vec{r}$ alone, and we denoted

$$d_{ee'}(\vec{\mathbf{r}})=\langle\chi_e(\vec{\mathbf{r}})|\mathbf{d}|\chi_{e'}(\vec{\mathbf{r}})\rangle=d^*_{e'e}(\vec{\mathbf{r}}). \tag{93}$$

In Eqs. (90)–(93), and henceforth, we let it be understood that all quantities pertain to the presence of a single perturber, unless otherwise indicated by a superscript (0) for zero perturbers.

A. Adiabatic approximation at the one-perturber level

We now neglect the fact that $\mathbf{T}_{nucl}$ induces transitions between different electronic states; that is, we approximate

$$\mathbf{H}|\chi_e(\vec{\mathbf{r}})\rangle=(\mathbf{T}_{nucl}+\mathbf{H}_{elec})|\chi_e(\vec{\mathbf{r}})\rangle \tag{94}$$

$$\simeq|\chi_e(\vec{\mathbf{r}})\rangle[\mathbf{T}_{nucl}+E_e(\vec{\mathbf{r}})]. \tag{95}$$

We thereby neglect $|\vec{\nabla}\chi_e(\vec{r})\rangle$, or equivalently approximate $\vec{\pi}_{ee'}(r)\simeq 0$. Denoting then

$$\mathbf{H}_e=\mathbf{T}_{nucl}+V_e(\vec{\mathbf{r}}) \tag{96}$$

with

$$V_e(\vec{\mathbf{r}})=E_e(\vec{\mathbf{r}})-E_e^\infty, \tag{97}$$

we get, for example,

$$\langle\chi_{e'}(\mathbf{r})|e^{is(\mathbf{H}-E_f)/\hbar}|\chi_{e''}(\vec{\mathbf{r}})\rangle\simeq\langle\chi_{e'}(\vec{\mathbf{r}})|\chi_{e''}(\vec{\mathbf{r}})\rangle e^{is\mathbf{H}_{e'}/\hbar} \tag{98}$$

$$=\delta_{e'e''}e^{is\mathbf{H}_{e'}/\hbar}. \tag{99}$$

Equation (92) becomes

$$\mathrm{Tr}\,e^{-\beta(\mathbf{H}-E_i)}\mathbf{d}_\alpha^\dagger(0)\mathbf{d}_\alpha(s)=\sum_{e\in\varepsilon_i}\sum_{e'\in\varepsilon_f}K_{ee'}(s), \tag{100}$$

where

$$K_{ee'}(s)=\mathrm{Tr}_r e^{-\beta\mathbf{H}_e}d_{ee'}(\vec{\mathbf{r}})e^{is\mathbf{H}_{e'}/\hbar}d_{e'e}(\vec{\mathbf{r}})e^{-is\mathbf{H}_e/\hbar}. \tag{101}$$

As shown numerically by Erikson and Sando [42], the adiabatic approximation done in this way at the one-perturber level does not seem to introduce errors that are too serious, contrary to doing it at the *N*-perturber level, which effectively constrains all binary collisions in a particular history to all lock onto the same pair potential curve. When the adiabatic approximation is done at the one-perturber level, a particular potential curve is selected only *within* each individual binary collision, but different *binary* collisions within a history choose pair potentials at random.

The main error expected from the above adiabatic approximation concerns the shift of the line center [20,43], which is largely due to weak collisions. These involve the merging region $r\simeq r_c$ in which transitions between different, but asymptotically equal, potential curves are easy due to their small separations. No great error is expected in the line wings (our main interest here), which are associated with transitions taking place when the perturber is traveling through regions where the potential curves are well separated.

B. Classical approximation

Let us rewrite Eq. (101) as

$$K_{ee'}(s)=\mathrm{Tr}_r e^{-(\beta/2)\mathbf{H}_e} d_{ee'}(\vec{\mathbf{r}}) e^{is\mathbf{H}_{e'}/\hbar} d_{e'e}(\vec{\mathbf{r}}) e^{-(\beta/2)\mathbf{H}_e} e^{-is\mathbf{H}_e/\hbar} \tag{102}$$

$$=\mathrm{Tr}_r e^{-(\beta/2)\mathbf{H}_e} d_{ee'}(\vec{\mathbf{r}}) e^{is\mathbf{H}_{e'}/\hbar} e^{-is\mathbf{H}_0/\hbar} e^{is\mathbf{H}_0/\hbar} d_{e'e}(\vec{\mathbf{r}}) e^{-(\beta/2)\mathbf{H}_e} e^{-is\mathbf{H}_0/\hbar} e^{is\mathbf{H}_0/\hbar} e^{-is\mathbf{H}_e/\hbar} \tag{103}$$

$$=\mathrm{Tr}_r e^{-(\beta/2)\mathbf{H}_e} d_{ee'}(\vec{\mathbf{r}}) \mathcal{T}_< \exp\left[\frac{i}{\hbar}\int_0^s dt V_{e'}(\vec{\mathbf{r}}_0(t))\right] d_{e'e}(\vec{\mathbf{r}}_0(s)) e^{-(\beta/2)[\mathbf{H}_0+V_e(\vec{\mathbf{r}}_0(s))]} \mathcal{T}_> \exp\left[\frac{-i}{\hbar}\int_0^s dt V_e(\vec{\mathbf{r}}_0(t))\right], \tag{104}$$

where we denoted

$$\vec{\mathbf{r}}_0(t)=e^{it\mathbf{H}_0/\hbar}\vec{\mathbf{r}}e^{-it\mathbf{H}_0/\hbar} \tag{105}$$

and

$$\mathbf{H}_0=\mathbf{T}_{nucl}=\frac{\vec{\mathbf{p}}^2}{2\mu}. \tag{106}$$

$\mathcal{T}_<$ and $\mathcal{T}_>$ are chronological operators, making time arguments increase from left to right ($<$) or from right to left ($>$). We next expand the trace Tr_r in terms of a complete set of normalized wave-packet states $|\vec{r}\vec{p}\rangle$, centered at $(\vec{r},\vec{p})$ in phase space, and satisfying

$$\langle\vec{r}\vec{p}|\vec{r}\vec{p}\rangle=1, \tag{107}$$

$$\frac{1}{(2\pi\hbar)^3}\int d\vec{r}d\vec{p}|\vec{r}\vec{p}\rangle\langle\vec{r}\vec{p}|=1. \tag{108}$$

For instance, $|\vec{r}\vec{p}\rangle$ may be a Gaussian wave packet. Under the action of $e^{-it\mathbf{H}_0/\hbar}$, the wave packet $|\vec{r}\vec{p}\rangle$ follows a straight trajectory,

$$e^{-(it\mathbf{H}_0/\hbar)}|\vec{r}\vec{p}\rangle=\left|\vec{r}+\frac{\vec{p}t}{\mu},\vec{p}\right\rangle \tag{109}$$

so that, for example,

$$\vec{\mathbf{r}}_0(t)|\vec{r}\vec{p}\rangle=e^{it\mathbf{H}_0/\hbar}\vec{\mathbf{r}}e^{-(it\mathbf{H}_0/\hbar)}|\vec{r}\vec{p}\rangle \tag{110}$$

$$=e^{it\mathbf{H}_0/\hbar}\vec{\mathbf{r}}\left|\vec{r}+\frac{\vec{p}t}{\mu},\vec{p}\right\rangle \tag{111}$$

$$\approx e^{it\mathbf{H}_0/\hbar}\left|\vec{r}+\frac{\vec{p}t}{\mu},\vec{p}\right\rangle\left(\vec{r}+\frac{\vec{p}t}{\mu}\right) \tag{112}$$

$$=|\vec{r}\vec{p}\rangle\left(\vec{r}+\frac{\vec{p}t}{\mu}\right). \tag{113}$$

In reality the packet in Eq. (109) spreads and acquires a phase [44], but these disappear in Eq. (113). We also have

$$e^{-(\beta/2)[\mathbf{H}_0+V_e(\vec{\mathbf{r}}_0(s))]}|\vec{r}\vec{p}\rangle\approx|\vec{r}\vec{p}\rangle e^{-(\beta/2)[\vec{p}^2/2\mu+V_e(\vec{r}+\vec{p}s/\mu)]} \tag{114}$$

so that

$$K_{ee'}(s)=\frac{1}{(2\pi\hbar)^3}\int d\vec{r}d\vec{p}e^{-\beta(\vec{p}^2/2\mu)}\tilde{d}_{ee'}(\vec{r}) \times\exp\left[\frac{i}{\hbar}\int_0^s dt V_{e'e}\left(\vec{r}+\frac{\vec{p}t}{\mu}\right)\right]\tilde{d}^*_{ee'}\left(\vec{r}+\frac{\vec{p}s}{\mu}\right), \tag{115}$$

where we defined

$$V_{e'e}(\vec{r})=V_{e'}(\vec{r})-V_e(\vec{r}), \tag{116}$$

$$\tilde{d}_{ee'}(\vec{r})=d_{ee'}(\vec{r})e^{-(\beta/2)V_e(\vec{r})}. \tag{117}$$

Putting this into Eq. (85) we get

$$g_\alpha(s)=\frac{1}{\int d\vec{p}e^{-\beta(\vec{p}^2/2\mu)}\sum_{e,e'}^{(\alpha)}|d_{ee'}|^2}\sum_{e,e'}^{(\alpha)}\int d\vec{r}d\vec{p}e^{-\beta(\vec{p}^2/2\mu)}\tilde{d}_{ee'}(\vec{r})\left\{\exp\left[\frac{i}{\hbar}\int_0^s dt V_{e'e}\left(\vec{r}+\frac{\vec{p}t}{\mu}\right)\right]\tilde{d}^*_{ee'}\left(\vec{r}+\frac{\vec{p}s}{\mu}\right)-\tilde{d}_{ee'}(\vec{r})\right\}. \tag{118}$$

We now assume that the perturbers have a single mean velocity $\overline{v}$, that is, in

$$\int d\vec{p}e^{-\beta(\vec{p}^2/2\mu)}=\int_0^\pi \sin\theta d\theta\int_0^{2\pi}d\phi\int_0^\infty p^2e^{-\beta(p^2/2\mu)}dp, \tag{119}$$

we put

$$p^2e^{-\beta p^2/2\mu}\approx(\mathrm{const})\,\delta(p-\mu\overline{v}). \tag{120}$$

The (const) appears in both the numerator and denominator of Eq. (118), and cancels out. We thus get, finally,

$$g_\alpha(s)=\frac{1}{\sum_{e,e'}^{(\alpha)}|d_{ee'}|^2}\sum_{e,e'}^{(\alpha)}\int_0^{+\infty}2\pi\rho d\rho\int_{-\infty}^{+\infty}dx\tilde{d}_{ee'}[r(0)]\left[\exp\left(\frac{i}{\hbar}\int_0^s dtV_{e'e}[r(t)]\right)\tilde{d}_{e'e}[r(s)]-\tilde{d}_{ee'}[r(0)]\right], \quad (121)$$

where $r(t)=[\rho^2+(x+\overline{v}t)^2]^{1/2}$ with ρ the impact parameter of the perturber trajectory.

In the above, we effectively neglected the influence of the potentials $V_e(r)$ and $V_{e'}(r)$ on the perturber trajectories, which remain straight lines. See Ref. [45] for a different derivation using WKB wave functions. This approximation should not cause errors that are too serious for the following reasons:

(i) The line center (shift and width) are mainly determined by the phase shifts associated with completed collisions, and should not be very sensitive, on average, to the details of trajectories.

(ii) The line wings, which *are* sensitive to what happens within collisions, are mainly determined by quasistatic effects, and the straight trajectory *classical* expression [Eq. (121)] yields, via a stationary phase approximation, the same quasistatic result as does the quantum expression, including the correct Boltzmann factors (see Ref. [45]).

Although we should really drop the Boltzmann factor $e^{-\beta V_e(r)}$ for consistency with our straight trajectories approximation, by keeping it we much improve the result in the wings. Note that over regions where $V_e(r)<0$, the factor $e^{-\beta V_e(r)}$ accounts for bound states of the radiator-perturber pair, but in a classical approximation wherein the discrete bound states are replaced by a continuum; thus, any band structure is smeared out. Note finally that we associated a factor $e^{-(1/2)\beta V_e(r)}$ with each factor d, rather than keeping $e^{-\beta V_e(r)}$ in a single piece associated with the first d only. This has the advantage of making the Boltzmann factor simply *modulate* $d(r)$. Also the resulting expression fits better with a Feynman path picture [45,46], since $e^{-(1/2)\beta V_e(r)}$ is the *amplitude* for the perturber to be at r, as opposed to the *probability* $e^{-\beta V_e(r)}$.

VI. APPLICATION TO THE LYMAN-α AND LYMAN-β PROFILES PERTURBED BY PROTONS

Since our main purpose in the present paper is to study the influence of dipole moment variations, the present calculations neglect the modulation of $d(\vec{r})$ by the Boltzmann amplitude $e^{-(1/2)\beta V_e(r)}$, which is different in emission and absorption. This is fairly justified if there are no bound states formed, which seems reasonable in the specific applications we have in view, and if we do not consider the very far wings involving very close collisions inside the repulsive core.

A. Diatomic potentials and dipole moments

The adiabatic interaction of a neutral hydrogen atom with a proton is described by potential energies $V(R)$ for each electronic state of the H_2^+ molecule. Electric-dipole transitions between these states are responsible for the line profile. When the difference $\Delta V(R)$ between the upper and lower potentials for a transition presents an extremum $\Delta V_{\rm ext}$ the unified theory predicts that there will be satellites periodically centered at [38,47,48]

$$\Delta\omega=k\Delta V_{\rm ext}, \quad k=1,2,3,\ldots. \quad (122)$$

Here $\Delta\omega$ is the frequency difference between the center of the unperturbed spectral line and the satellite feature, measured for convenience in the same units as the potential-energy difference.

An H_2^+ correlation diagram is given in Ref. [23] for Lyman-α and in Ref. [49] for Lyman-β. We used the potentials of H_2^+ calculated by Madsen and Peek [31] for the transitions contributing to Lyman-α and Lyman-β; that is, for those which asymptotically go, respectively, to the $n=2$ and $n=3$ state of atomic hydrogen and a free proton. The existence of minima in the potential differences for some allowed transitions leads us to expect the presence of satellite features on the wings of Lyman-α and Lyman-β [23,49]. For the transition $2p\sigma_u-3d\sigma_g$ the difference potential minimum is $-11\,080$ cm^{-1}, which gives rise to a binary satellite at 1405 Å in the red wing of Lyman-α. This feature has been observed in UV spectra of DA white dwarfs and laser-produced plasmas. For these very low densities the strength of the wing up to the binary satellite is linear with density.

Dipole transition moments have been calculated by Ramaker and Peek [32]. To point out the importance of the variation of dipole moments we display its variation with internuclear distance. Figures 1 and 2 show the dipole moment for the transitions that should produce a satellite on Lyman-α at 1405 Å and on Lyman-β at 1078 Å. The last one is due to the transition $5g\sigma_g-2p\sigma_u$. It has been observed in DA white dwarf spectra obtained with HUT [13].

The transition moment at small internuclear distances differs notably from the asymptotic value, in particular for R around the potential minimum where the satellite is formed. This behavior leads us to expect that the variation of the dipole will have an important effect on the amplitude of the 1405 Å satellite. By contrast, in Fig. 3 the dipole moment for a transition contributing to Lyman-α at 1234 Å remains flat with a value close to the asymptotic dipole.

B. Calculation of the Lyman-α and Lyman-β profiles

Figure 4 compares the profiles obtained in the constant dipole approximation to the new calculations which take into account the variation of the dipole during collisions. The amplitude of the 1405 Å satellite is seen to be roughly mul-

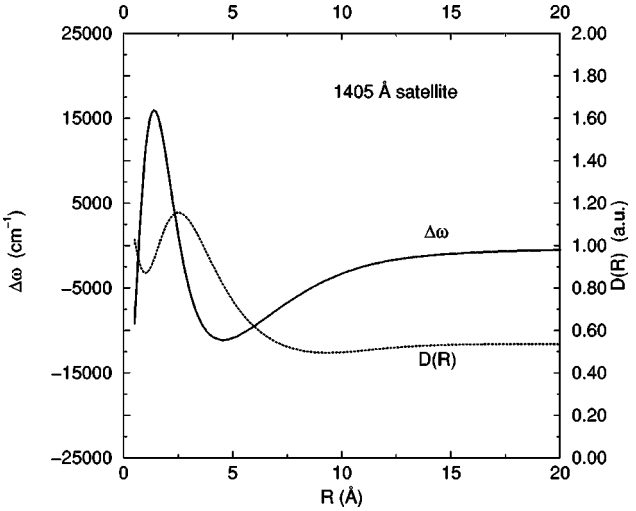

FIG. 1. Difference potential energy in cm^{-1} and the corresponding $D(R)$ in atomic units for the 1405 Å satellite of Lyman-α.

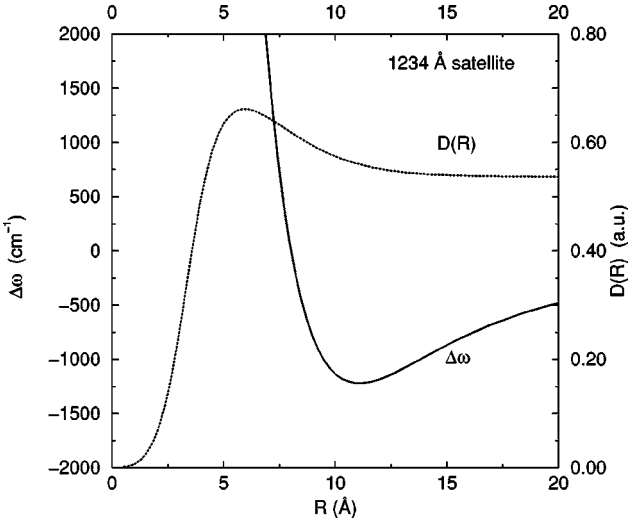

FIG. 3. Difference potential energy in cm^{-1} and the corresponding $D(R)$ in a.u. for the 1234 Å satellite of Lyman-α.

tiplied by a factor of 2, whereas the other satellites in the wing have not changed much because their dipole moments stay close to the asymptotic values and do not vary as dramatically in the region of interest. Because of the overlap of the Lyman-α blue wing and the Lyman-β red wing we present the sum of the profiles of Lyman-α and Lyman-β in Fig. 5. The variation of dipoles also affects the amplitude of the satellites present in the Lyman-β red wing [49].

VII. APPLICATION TO LASER-PRODUCED HYDROGEN PLASMA

The observation of the shape and far wing of Lyman-α broadened by neutral atom and ion collisions in a laser-produced hydrogen plasma also has been compared with some of the calculations discussed here [29]. In those experiments, self-focusing of a 1.064 μm, 6 ns, 600 mJ laser caused most of its energy to be delivered suddenly to a cylindrical volume only a few μm in diameter and a few mm long. The resulting shock front and postshock gas provide a source for studying radiative collisions of atomic H experimentally with time-resolved emission spectroscopy. The prompt atomic emission from the plasma arose from a thin hot expanding shell in which the primary components were neutral H, H^+, and electrons. The observed spectrum revealed satellites due to collisions with H and H^+, including strong satellites close to Lyman-α at 1230 and 1240 Å, and weaker ones in the extremely far wing at 1400 and 1600 Å.

The satellite observed at approximately 1230 Å was identified as due to collisions with H^+. Figure 3 illustrates that the difference potential minimum contributing to this feature occurs at an atom-ion separation of 10 Å, and as such is a probable collision in a dense plasma. This satellite dominates the near wing of Lyman-α in the observed spectrum, as the theoretical profiles predict. The spectral region close to the line core was modified by radiation transfer effects and collisions with electrons in the plasma source. In the far wing around 1600 Å, however, the observed profile

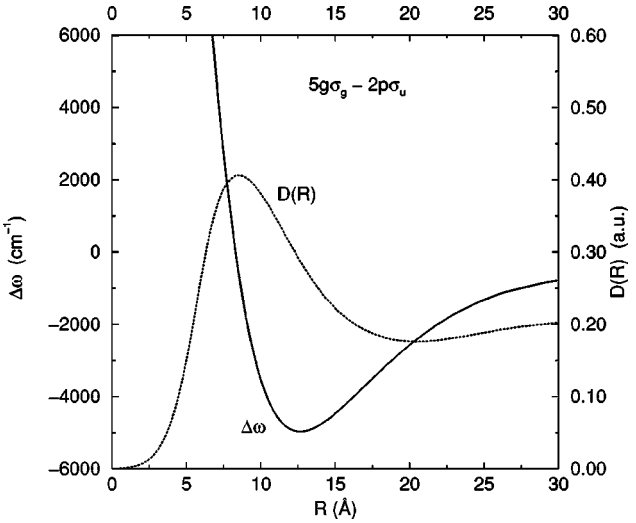

FIG. 2. Variation of the dipole moments with internuclear distance for one of the main transitions contributing to the red wing of Lyman-β.

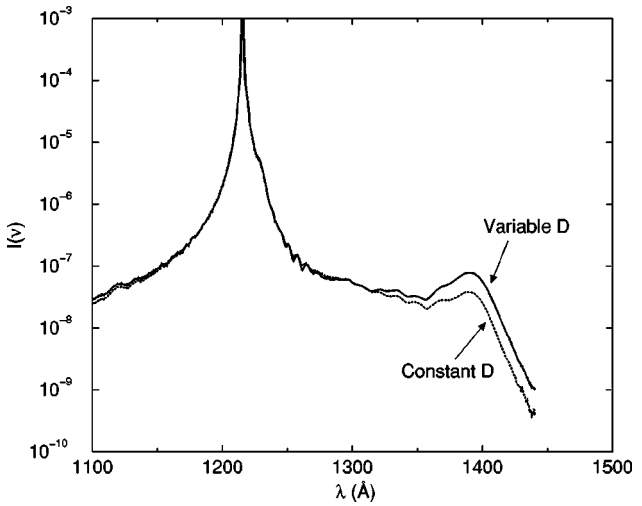

FIG. 4. Comparison of Lyman-α profiles with and without variation of dipole moments. $I(\nu)$ is normalized so that $\int I(\nu)d\nu = 1$.

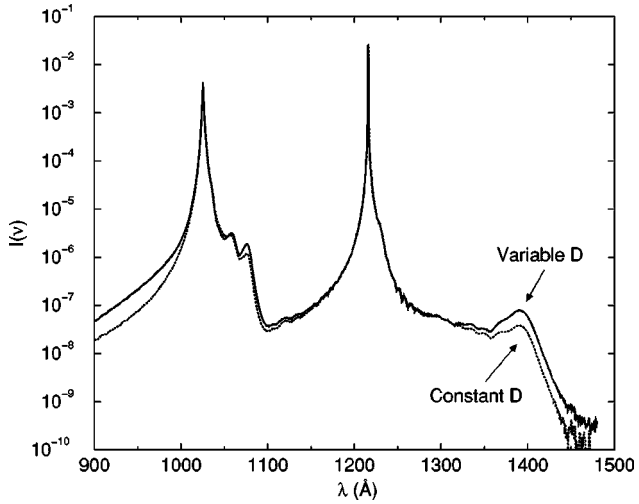

FIG. 5. Profile of the sum of Lyman-α and Lyman-β. $I(\nu)$ is normalized as in Fig. 4.

was optically thin and it was possible to make a quantitative comparison with the theory. The result is reproduced in Fig. 6, in which the experimental profile has been corrected for bound-bound emission. The theory described here allows for the increase in the dipole moment at the atom-atom separations contributing to this region of the spectrum. It predicts a satellite which is about a factor of two more intense at 1600 Å, relative to the continuum at 1500 Å, than a constant dipole theory. As the figure shows, the variable dipole model is in much better agreement with the experiment.

Both theory and experiment show an oscillatory structure between the satellite and the line, with a minimum at about 1525 Å. These oscillations are an interference effect [45,50], and are expected to depend on the relative velocity of the collision and therefore on temperature. For this reason, we investigated the effect of averaging over velocity in the theoretical evaluation, rather than using a single fixed mean

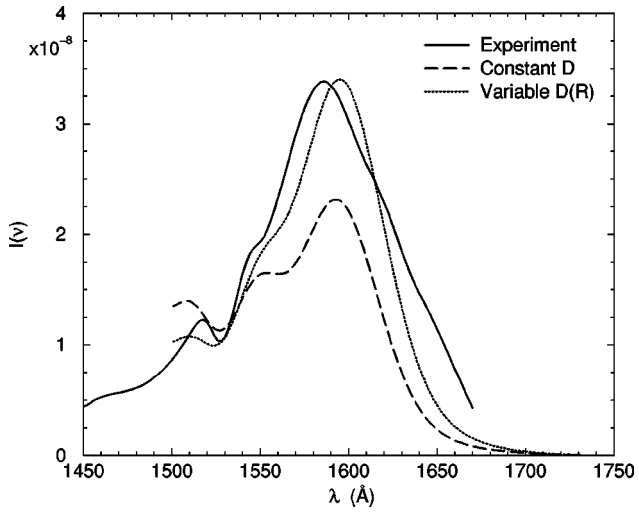

FIG. 6. Comparison of the observed 1600 Å region with theoretical profiles with and without the variation of dipole moment. The experiment is a measurement of the optically thin emission from atomic hydrogen compressed and heated by the shock wave from a laser-produced plasma at a neutral density of approximately 10^{19} atoms/cm^3.

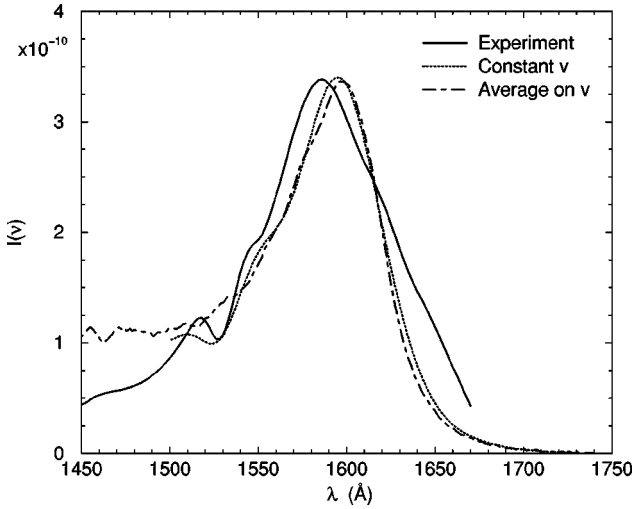

FIG. 7. Velocity average for the 1600 Å satellite of Lyman-α computed for 10 000 K with $n_H = 10^{17}$ cm^{-3} compared to a a laser-plasma experiment at $n_H = 10^{19}$ cm^{-3} scaled to fit.

velocity. The evaluation was done numerically by performing the calculation for different velocities and then thermally averaging with 24-point Gauss-Laguerre integration. The result for a single trial temperature of 10 000 K is shown in Fig. 7. Both the constant and variable dipole moment theories predicted an oscillation at 1530 Å with a depth of about 20% of the continuum. The velocity averaging reduces this to about 5%. The velocity-averaged profile including a variable dipole moment is still in good agreement with the experiment. Averaging over velocity does not significantly change the far wing profile, as one would expect.

VIII. ASTROPHYSICAL APPLICATION

A. Comparison of IUE observation of λ Bootis star with synthetic spectra

Satellite features at 1600 and 1405 Å in the Lyman-α wing associated with free-free quasimolecular transitions of H_2 and H_2^+ have been observed in UV spectra of certain stars obtained with the IUE and Hubble Space Telescope (HST) [24–27]. The stars that show Lyman-α satellites are DA white dwarfs, old *Horizontal Branch* stars of spectral type A, peculiar spectral type *A* stars of Population I, and the λ Bootis stars. The last two have the distinctive property of poor *metal* content, that is, low abundances of elements other than H and He. In the observed UV spectra of DA white dwarf stars, λ Bootis stars, and laboratory plasmas, the strength of the contributions to the Lyman-α wing caused by neutral collisions relative to the contributions caused by charged perturbers depends very strongly on the ionization balance of hydrogen, and thus, through the Saha equation, on the stellar parameters $T_{\rm eff}$ and $\log_{10} g$. As a consequence of its dependence on the degree of ionization, the shape of the Lyman-α wing is a very sensitive tool for determining these parameters once accurate absorption coefficients for the line wing are known.

The new theoretical Lyman-α line profiles have been included in stellar atmosphere programs for the computation of model stellar atmosphere spectra and synthetic spectra of λ Bootis stars [51,52]. A comparison of the new calculations

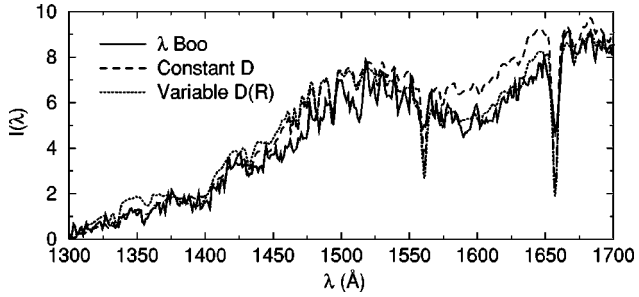

FIG. 8. Comparison of synthetic spectra with and without the variation of dipole moment and the IUE spectrum of λ Bootis.

with observations made with the IUE as shown in Fig. 8 demonstrates that these last improvements are of fundamental importance for obtaining a better quantitative interpretation of the spectra and for determining stellar atmospheric parameters.

B. Comparison with a HUT observation of the white dwarf Wolf 1346

The optical spectrum of the star Wolf 1346 shows that it is a normal type DA white dwarf with a temperature of 20 000 K and no indications of chemical elements other than hydrogen. While several hotter DA white dwarfs show a Lyman series compatible with symmetrically Stark broadened profiles without unexplained features, Wolf 1346 has a Lyman-β line with a strong asymmetry, a very steep red wing, and absorption features in the wing near 1060 and 1078 Å. In Fig. 9 the comparison for the HUT spectrum of Wolf 1346 shows that the far UV is very well fitted with a synthetic spectrum computed with the profile calculations described here [53].

IX. CONCLUSION

The main objective of this paper was to show the influence of the variation of the dipole moment on line profile features that are present in the far wings of the Lyman series lines of atomic H. We first provided a careful derivation of an adiabatic classical path approximation for the spectrum, allowing for degenerate atomic states and radiative dipole moments which vary with internuclear distances.

In order to take into account the overlap of the Lyman-α blue wing and the Lyman-β red wing we had to sum correctly their respective contributions. Figure 5 illustrates a numerical calculation of the far ultraviolet profile of Lyman-α and Lyman-β based on the theory presented here. Large changes in the intensity of the satellites occur when the dipole moment varies significantly in the region of internuclear distance where the satellite is formed. As a consequence the

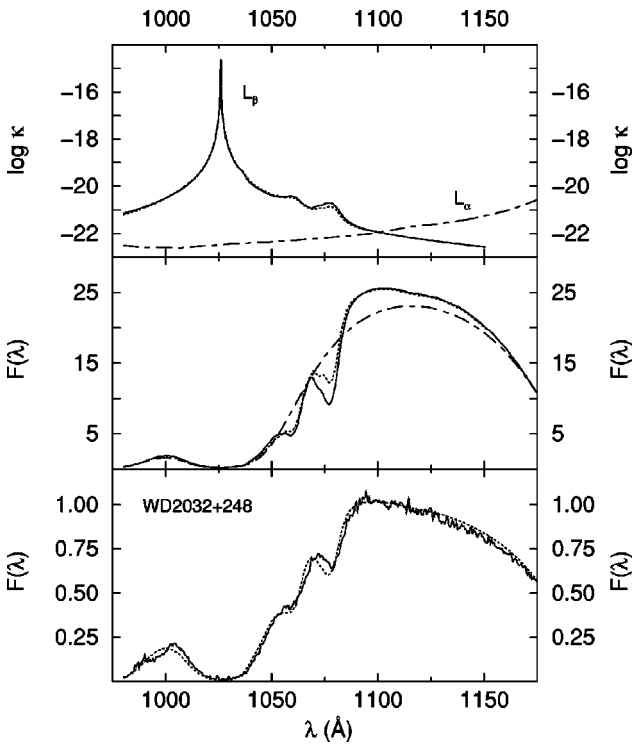

FIG. 9. Upper panel: absorption coefficient per hydrogen atom in the ground state due to Lyman-β (left) and Lyman-α (right, dotted-dashed line). New line profiles with variable dipole moments for Lyman-β are drawn with a solid line, and old calculations are the dotted line. The density of perturbers (protons) is 10^{16} cm^{-3}. The temperature assumed for the calculation is 20 000 K; the profile, however, is very insensitive to the temperature. Middle panel: theoretical synthetic spectra for a pure hydrogen white dwarf model atmosphere with $T_{\rm eff}=18\,000$, $\log_{10} g=8$. Ordinate is F_λ in units of 10^{16} erg cm^{-2} s^{-1}. The solid line is calculated with the new profiles, the dotted lines with the old profiles with constant dipole moments, and the dashed line is a synthetic spectrum calculated with the standard VCS Stark broadening theory. Lower panel: far UV spectrum of the white dwarf WD2032+248 (Wolf 1346) observed with the Hopkins Ultraviolet Telescope (solid line), and theoretical model (dotted line).

variation of the dipole has to be taken into account to obtain reliable results if they are used as diagnostics of stellar and plasma parameters.

ACKNOWLEDGMENT

The work at the University of Louisville is supported by a grant from the U.S. Department of Energy, Office of Science, Office of Basic Energy Sciences, Division of Chemical Sciences.

[1] P. W. Anderson and J. D. Talman, Bell System, Murray Hill, NJ, Technical Report No. 3117 (unpublished).

[2] A. Gallagher, in *Atomic, Molecular, & Optical Physics Handbook*, edited by G. W. F. Drake (AIP Press, Woodbury, New York, 1996), p. 220.

[3] M. Lapp, Phys. Lett. **23**, 553 (1966).

[4] J. A. Gwinn, P. M. Thomas, and J. F. Kielkopf, J. Chem. Phys. **48**, 568 (1968).

[5] A. Tam, G. Moe, W. Park, and W. Happer, Phys. Rev. Lett. **35**, 85 (1975).

[6] A. Gallagher and T. Holstein, Phys. Rev. A **16**, 2413 (1977).
[7] W.-Ü. L. Tchang-Brillet, A. Spielfiedel, N. Feautrier, and D. Haner, J. Phys. B **22**, 3915 (1989).
[8] N. F. Allard and J. F. Kielkopf, Rev. Mod. Phys. **54**, 1103 (1982).
[9] J. C. Stewart, J. M. Peek, and J. Cooper, Astrophys. J. **l179**, 983 (1973).
[10] K. M. Sando, R. O. Doyle, and A. Dalgarno, Astrophys. J. **157**, L143 (1969).
[11] E. P. Nelan and G. Wegner, Astrophys. J. **289**, L31 (1985).
[12] D. Koester, E.-M. Weideman, K. Zeidler, and G. Vauclair, Astron. Astrophys. **142**, L5 (1985).
[13] D. Koester *et al.*, Astrophys. J. **463**, L93 (1996).
[14] B. Hansen, Nature (London) **394**, 860 (1998).
[15] H. Richer, Nature (London) **394**, 825 (1998).
[16] M. Baranger, Phys. Rev. **111**, 481 (1958).
[17] M. Baranger, Phys. Rev. **111**, 494 (1958).
[18] A. Royer, Can. J. Phys. **52**, 1816 (1974).
[19] A. Royer, Phys. Rev. A **22**, 1625 (1980).
[20] W. C. Kreye and J. F. Kielkopf, J. Phys. B **30**, 2075 (1997).
[21] N. F. Allard and J. F. Kielkopf, Astron. Astrophys. **242**, 133 (1991).
[22] N. F. Allard and D. Koester, Astron. Astrophys. **258**, 464 (1992).
[23] N. F. Allard, D. Koester, N. Feautrier, and A. Spielfiedel, Astron. Astrophys. Suppl. **200**, 58 (1994).
[24] D. Koester and N. F. Allard, in *White Dwarfs: Advances in Observation and Theory*, edited by M. Barstow (Kluwer, Dordrecht, 1993), p. 237.
[25] D. Koester, N. F. Allard, and G. Vauclair, Astron. Astrophys. **291**, L9 (1994).
[26] H. Holweger, D. Koester, and N. F. Allard, Astron. Astrophys. **290**, L21 (1994).
[27] P. Bergeron, F. Wesemael, R. Lamontagne, G. Fontaine, R. Saffer, and N. F. Allard, Astrophys. J. **449**, 258 (1995).
[28] J. F. Kielkopf and N. F. Allard, Astrophys. J. **450**, L75 (1995).
[29] J. F. Kielkopf and N. F. Allard, Phys. Rev. A **58**, 4416 (1998).
[30] A. Royer, Phys. Rev. A **3**, 2044 (1971).
[31] M. M. Madsen and J. M. Peek, At. Data **2**, 171 (1971).
[32] D. E. Ramaker and J. M. Peek, J. Phys. B **5**, 2175 (1972).
[33] T. E. Sharp, At. Data **2**, 119 (1971).
[34] L. Wolniewicz and K. Dressler, J. Chem. Phys. **88**, 3861 (1988).
[35] K. Dressler and L. Wolniewicz, J. Chem. Phys. **82**, 4720 (1985).
[36] I. Drira, J. Mol. Spectrosc. (to be published).
[37] I. I. Sobel'man, *Introduction to the Theory of Atomic Spectra* (Pergamon Press, Oxford, 1972), p. 293.
[38] A. Royer, Acta Phys. Pol. A **54**, 805 (1978).
[39] F. T. Smith, Phys. Rev. **179**, 111 (1969).
[40] P. Julienne and F. Mies, Phys. Rev. A **30**, 831 (1984).
[41] A. Spielfiedel and N. Feautrier, J. Phys. B **22**, 3227 (1989).
[42] G. Erikson and K. Sando, Phys. Rev. A **22**, 1500 (1980).
[43] A. Spielfiedel, D. Gilbert, E. Roueff, and F. Rostas, J. Phys. B **12**, 22 (1979).
[44] R. G. Littlejohn, Phys. Rep. **13**, 193 (1986).
[45] A. Royer, Phys. Rev. A **4**, 499 (1971).
[46] A. Royer, Acta Phys. Pol. A **50**, 289 (1976).
[47] N. F. Allard, J. Phys. B **11**, 1383 (1978).
[48] J. F. Kielkopf and N. F. Allard, Phys. Rev. Lett. **43**, 196 (1979).
[49] N. F. Allard, J. F. Kielkopf, and N. Feautrier, Astron. Astrophys. **330**, 782 (1998).
[50] K. M. Sando and J. G. Wormhoudt, Phys. Rev. A **7**, 1889 (1973).
[51] N. F. Allard, R. L. Kurucz, M. Gerbaldi, and R. Faraggiana, in *UV Astrophysics Beyond the IUE Final Archive, Sevilla, 1997, ESA-SP413* (ESA, ESTEC, Noordwik, The Netherlands, 1998).
[52] N. F. Allard, I. Drira, M. Gerbaldi, J. F. Kielkoff, and A. Spielfiedel, Astron. Astrophys. **335**, 1124 (1998).
[53] D. Koester, V. Sperhake, N. F. Allard, D. S. Finley, and S. Jordan, Astron. Astrophys. **336**, 276 (1998).